Journal of Materials Chemistry B

ROYAL SOCIETY OF CHEMISTRY

PAPER

View Article Online
View Journal | View Issue

Cite this: J. Mater. Chem. B, 2022, 10, 7628

A Cu-based nanoplatform for near-infrared light amplified multi-mode prostate cancer specific therapy†

Bo Xu,[a] Rui Niu,[b] Ying Tang,[c] Chunxi Wang,*[a] Longhai Jin *[d] and Yinghui Wang [b]

Received 25th May 2022,
Accepted 18th July 2022

DOI: 10.1039/d2tb01109c

rsc.li/materials-b

Chemodynamic therapy (CDT), as a new method for oncotherapy, can convert less reactive hydrogen peroxide (H_2O_2) into highly toxic hydroxyl radicals (•OH) in the tumor microenvironment (TME) to kill tumor cells and inhibit tumor growth. However, the TME usually presents a low content of endogenous H_2O_2 and weak acidity, which weakens the therapeutic effect of CDT to a certain extent. Here, we developed a multifunctional nanoplatform based on Cu-doped mesoporous carbon nanospheres loaded with free radical generator 2′-azobis[2-(2-imidazolin-2-yl)propane]-dihydrochloride (AIPH) and polyacrylic acid (Cu-MNCS-AIPH@PAA). Cu-MNCS-AIPH@PAA exhibited high photothermal conversion efficiency, and could not only act as a good photothermal agent for photothermal therapy (PTT) but also trigger AIPH to produce alkyl radicals. In response to the specificity of the TME, Cu-MNCS-AIPH@PAA could generate •OH through a Fenton-like reaction for CDT and enhance the efficacy of CDT by a photothermal effect. The excellent anticancer efficiency by the synergistic effect of CDT, PTT and free radicals, high biocompatibility and low adverse effects of Cu-MNCS-AIPH@PAA make it an ideal nanoplatform for tumor therapy.

Introduction

Prostate cancer (PCa) is the most frequent malignancy of the male genitourinary system, and its morbidity ranks second in all masculine malignancies worldwide according to GLOBOCAN statistics of the World Health Organization (WHO) in 2020.[1–3] Although conventional tumor treatments have been widely applied for PCa therapy, such as surgery, radiotherapy, chemotherapy and endocrine therapy, these treatments all have their own disadvantages, including limited treatment effect, serious adverse effects, and so on.[4–7] Therefore, it is imperative to explore a new, safe, and effective treatment method for PCa. Recently, chemodynamic therapy (CDT) as a new method for oncotherapy has attracted more attention,[8–10] which utilizes Fenton or Fenton-like reactions to convert less reactive hydrogen peroxide (H_2O_2) into highly cytotoxic hydroxyl radicals (•OH) in the tumor microenvironment (TME) for killing tumor cells and inhibiting tumor growth.[11–16] Compared with other treatments, CDT can specifically kill cancer cells without significant toxicity to normal tissues by initiating chemical reactions in the TME.[17–20] CDT mediated by various transition metals (such as Fe, Cu, Co, *etc.*) has been widely used in nanocatalytic tumor therapy.[21–27] Although the Cu-based Fenton-like reaction has a much greater reaction rate than the Fenton reaction,[28,29] the low content of endogenous H_2O_2 in the TME weakens the therapeutic effect of CDT.

[a] Department of Urology, The First Hospital of Jilin University, Changchun 130021, Jilin, China. E-mail: chunxi@jlu.edu.cn
[b] State Key Laboratory of Rare Earth Resource Utilization, Changchun Institute of Applied Chemistry (CIAC), Chinese Academy of Sciences, Changchun 130022, China
[c] Department of Gastroenterology, The First Hospital of Jilin University, Changchun 130021, Jilin, China
[d] Department of Radiology, The Second Hospital of Jilin University, Changchun 130041, Jilin, China. E-mail: jinlonghai@jlu.edu.cn

† Electronic supplementary information (ESI) available. See DOI: https://doi.org/10.1039/d2tb01109c

Longhai Jin

Longhai Jin received his PhD degree in medicine from Jilin University in 2018. He is working as an attending physician at the Second Hospital of Jilin University. His research interest focuses on the synthesis and bioapplication of multifunctional nanomaterials.

Photothermal therapy (PTT) is an effective and new therapeutic modality for malignant tumors, which utilizes photothermal agents to convert near-infrared (NIR) light energy into heat energy.[30–32] PTT can not only inhibit the tumor growth by accurately formulating individual treatment plans through flexibly adjusting the irradiation area, time and energy, but also improve the efficiency of Fenton or Fenton-like reactions.[33–44] Recently, drugs that respond to external stimulation to produce highly cytotoxic free radicals in the hypoxic tumor microenvironment have attracted wide attention for greatly improving the anti-tumor therapeutic effect.[45,46] For example, 2,2′-azobis[2-(2-imidazolin-2-yl)propane]-dihydrochloride (AIPH), as a superior water-soluble azo compound,[47–51] could be rapidly decomposed triggered by the photothermal effect to generate alkyl radicals without O_2 and H_2O_2,[52] which has become a research hotspot for tumor therapy. Therefore, it is a promising strategy to construct a Cu-based Fenton agent with good photothermal effect and drug delivery ability for highly effective treatment of PCa.

Building from these ideas, we constructed a multifunctional nanoplatform based on polyacrylic acid (PAA)-modified Cu-doped mesoporous carbon nanospheres to load AIPH (Cu-MNCS-AIPH@PAA) for highly efficient stimuli-responsive PCa therapy with low adverse effects (Scheme 1). Due to the strong absorption in the NIR region, Cu-MNCS-AIPH@PAA exhibited high photothermal conversion efficiency, which could not only act as a good photothermal agent for PTT, but also trigger AIPH to produce alkyl radicals. In response to the specificity of the TME, including low content of endogenous H_2O_2 and mild acidity, Cu-MNCS-AIPH@PAA could generate $^{\bullet}OH$ through a Fenton-like reaction for CDT, and its efficacy was further improved by the photothermal effect. The good anticancer effect of Cu-MNCS-AIPH@PAA was demonstrated *in vitro* and *in vivo* by a synergistic effect of CDT, PTT, and alkyl radicals. Therefore, Cu-MNCS-AIPH@PAA is a promising nanoplatform for PCa therapy with good biocompatibility, excellent anticancer efficiency and low adverse effects.

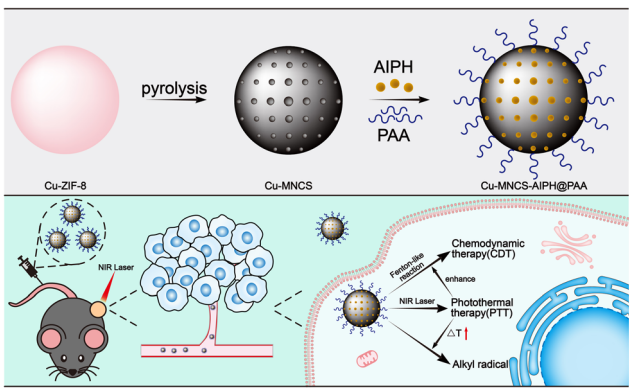

Scheme 1 Schematic illustration of the construction and anticancer treatment mechanism of Cu-MNCS-AIPH@PAA nanoparticles.

Results and discussion

The design and synthesis process of Cu-MNCS-AIPH@PAA was described in detail, as shown in Scheme 1. Scanning electron microscope (SEM) and transmission electron microscope (TEM) images indicated that the average size of the Cu-MNCS was about 200 nm, and the element mapping images displayed the uniform distribution of Cu, C, N, and O elements (Fig. 1a–e and Fig. S1, S2, ESI†). The X-ray diffraction (XRD) image showed that the diffraction peaks at 43.5°, 50.6°, and 74.3° were consistent with the standard card of face-centered cubic Cu (JCPDS No. 04-0836), and the broad peak at 25.2° was attributed to the diffraction peak of graphite (Fig. 1f).[53] The X-ray photoelectron spectroscopy (XPS) results further confirmed the element composition and valence state of Cu-MNCS (Fig. S3, ESI†). The spectrum of Cu 2p showed that the low-energy band was made up of two peaks at 932.6 eV (Cu^0) and 933.5 eV (Cu^{2+}) and the high-energy band was also composed of two peaks centered at 952.4 eV (Cu^0) and 953.5 eV (Cu^{2+}) (Fig. 1g).[54] The spectrum of N 1s (Fig. S4, ESI†) showed four binding energy peaks at 403.31 eV (graphitic N), 400.99 eV (Cu–N), 399.56 eV (pyrrolic N) and 398.45 eV (pyridinic N).[55] All these results indicated the successful synthesis of Cu-MNCS. The

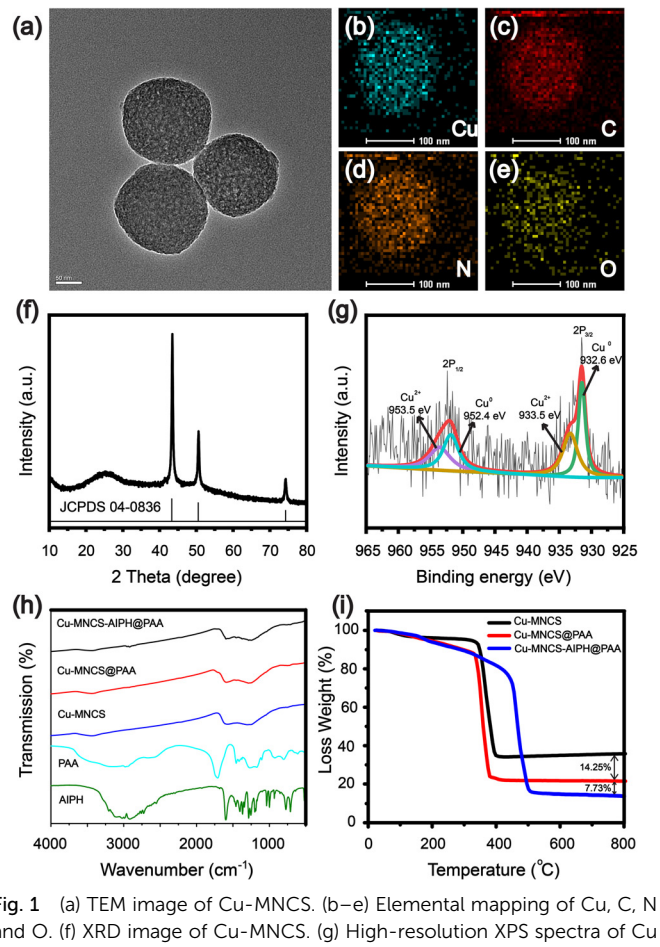

Fig. 1 (a) TEM image of Cu-MNCS. (b–e) Elemental mapping of Cu, C, N and O. (f) XRD image of Cu-MNCS. (g) High-resolution XPS spectra of Cu 2p. (h) FTIR spectra of AIPH, PAA, Cu-MNCS, Cu-MNCS@PAA and Cu-MNCS-AIPH@PAA. (i) Thermogravimetric analysis curves of Cu-MNCS, Cu-MNCS@PAA, and Cu-MNCS-AIPH@PAA.

Brunauer–Emmett–Teller (BET) result showed the typical mesoporous structure of Cu-MNCS, endowing it with great capacity as a drug carrier (Fig. S5, ESI†). Then, AIPH was loaded into Cu-MNCS, and further functionalized by PAA. As shown in Fig. 1h, the existence of the bands at 3385 and 1718 cm^{-1} attributed to AIPH and PAA in the FT-IR spectrum of Cu-MNCS-AIPH@PAA indicated the successful loading of AIPH and modification of PAA. The zeta potential changes at different preparation steps confirmed the successful preparation of Cu-MNCS-AIPH@PAA (Fig. S6, ESI†). The loading efficiency of AIPH was calculated to be about 7.73% according to the thermogravimetric curves, implying that Cu-MNCS could act as a promising carrier for AIPH (Fig. 1i).

The ultraviolet-visible spectroscopy (UV-vis) absorption spectrum of Cu-MNCS@PAA showed absorption in the NIR region, making it a prospective photothermal agent for PTT (Fig. S7, ESI†). The photothermal performances of Cu-MNCS@PAA were further investigated by a thermal imaging camera to detect its temperature variations. After irradiation with an 808 nm laser (0.7 W cm^{-2}) for 10 min, the temperature of a Cu-MNCS@PAA aqueous solution increased by 24.1 °C when its concentration reached 80 μg mL^{-1} (Fig. 2a and b). In contrast, under the same conditions, the temperature of water only increased by 1.2 °C (Fig. 2c). The photothermal conversion efficiency of Cu-MNCS@PAA was calculated to be 42.4%, indicating that Cu-MNCS@PAA had good photothermal properties (Fig. 2d). The UV-vis absorption spectra of Cu-MNCS@PAA remained unchanged before and after 808 nm laser irradiation, which showed the good photothermal stability of Cu-MNCS@PAA (Fig. 2e). It was further proved by the unchanged temperature curve after five on-off cycle processes (Fig. 2f). These results demonstrated that Cu-MNCS@PAA had great prospects as a photothermal agent for PTT.

The •OH generation ability of Cu-MNCS@PAA was evaluated by using terephthalic acid (TA) as a probe that emitted fluorescence at 430 nm in response to •OH. As shown in Fig. 3a, compared with the TA and TA + H_2O_2 groups, the Cu-MNCS@PAA group showed obvious emission in different conditions (pH = 4.0, 5.0 and 6.5, respectively). The results indicated that the generation of •OH through a Fenton-like reaction was pH-dependent. At the same time, the fluorescence intensity significantly increased as the temperature increased and under irradiation with an 808 nm laser, indicating that high temperature could also accelerate the reaction rate of the Fenton-like reaction by promoting the ionization process (Fig. 3b and Fig. S8, ESI†).

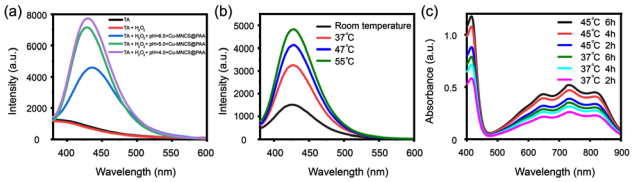

Fig. 3 (a) Fluorescence spectra of terephthalic acid oxidized by Cu-MNCS@PAA in the presence of H_2O_2 at different pH values. (b) Fluorescence spectra of terephthalic acid oxidized by Cu-MNCS@PAA in the presence of H_2O_2 at pH = 6.5 and different temperatures. (c) Generation of $ABTS^{+\bullet}$ as triggered by Cu-MNCS-AIPH@PAA at different temperatures and time.

Then, we further investigated the alkyl radical production ability of Cu-MNCS-AIPH@PAA by using 2,2'-azino-bis (3-ethylbenzothiazoline-6-sulfonic acid (ABTS) as an indicator. $ABTS^{+\bullet}$ was the product of the reaction between ABTS and the alkyl radical and presented a classic absorbance in a UV-vis spectrometer. As shown in Fig. 3c, when ABTS was treated with Cu-MNCS-AIPH@PAA, the absorbance intensity of $ABTS^{+\bullet}$ enhanced with the extension of the incubation time and temperature rise, indicating that the thermal effect could improve the decomposition of AIPH. The good •OH and alkyl radical production ability endowed Cu-MNCS-AIPH@PAA with great potential for the therapy of PCa.

The biocompatibility and therapeutic efficiency of Cu-MNCS-AIPH@PAA on mouse prostate cancer RM-1 cells were assessed using the Cell Counting Kit-8 (CCK-8) assay. The cell viability was still more than 87% when the concentration of Cu-MNCS-AIPH@PAA reached 100 μg mL^{-1} (Fig. 4a), implying its good biocompatibility. In simulated TME, the cell viability of the Cu-MNCS@PAA group declined with the concentration increasing, ascribed to the •OH generation through Fenton-like reaction (Fig. 4b). After irradiation with an 808 nm laser, the killing cancer cell ability was obviously improved owing to the synergistic effect of PTT and the photothermal effect improved CDT. After loading AIPH, the Cu-MNCS-AIPH@PAA + laser group exhibited a good inhibition effect of RM-1 cells due to the alkyl radical generation in normal conditions. Compared to other groups, the Cu-MNCS-AIPH@PAA + laser group showed the best anticancer effect in simulated TME owing to the combination of PTT, CDT, and alkyl radical generation triggered by the photothermal effect. These results were consistent with those of calcein AM and propidium iodide (PI) staining (Fig. 4c). To further confirm the free radical generation, 2′,7′-dichlorofluorescein diacetate (DCFH-DA), which could be oxidized by free radicals,

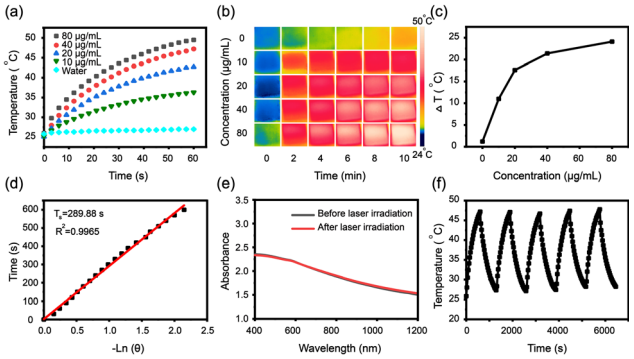

Fig. 2 (a) Temperature curve of Cu-MNCS@PAA with different concentrations under irradiation (808 nm, 0.7 W cm^{-2}). (b) Infrared thermal images with changeable concentrations. (c) ΔT of Cu-MNCS@PAA with increasing concentration. (d) Cooling time graph *versus* − Ln(θ) acquired from the cooling stage. (e) The UV-vis spectrum of Cu-MNCS@PAA (40 μg mL^{-1}) before and after 808 nm laser irradiation. (f) Temperature changes for five cycles of Cu-MNCS@PAA (40 μg mL^{-1}) under an 808 nm laser for 10 min.

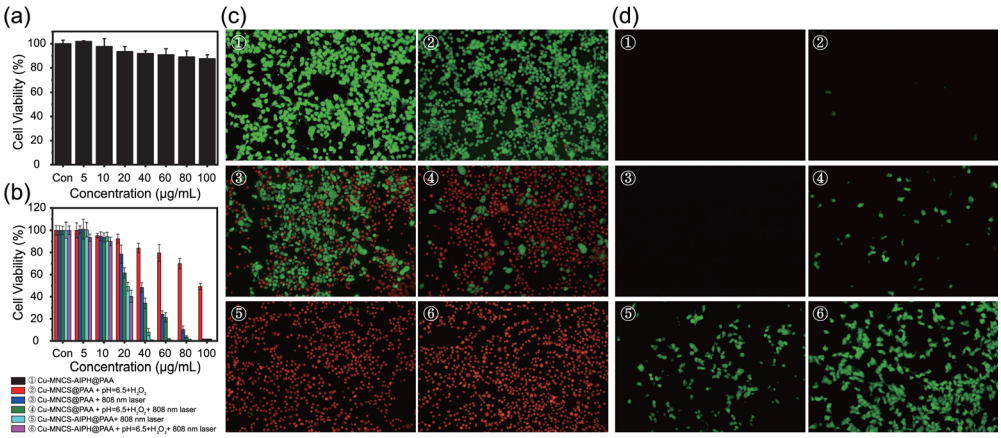

Fig. 4 (a and b) Cell viability of RM-1 cells treated with different concentrations of the nanoparticles (0, 5, 10, 20, 40, 80 and 100 μg mL^{-1}) for 24 h. (c) Fluorescence images of RM-1 cells stained with Calcein AM and PI after different treatments. (d) Fluorescence images of RM-1 cells stained with DCFH-DA after different treatments.

was used as the fluorescent probe to evaluate the free radical production in RM-1 cells. In contrast to the Cu-MNCS-@PAA and Cu-MNCS-@PAA + laser group, weak green emission could be observed in the Cu-MNCS-@PAA group in the TME, indicating the •OH generation through the Fenton-like reaction (Fig. 4d). The intensity of green fluorescence after irradiation with an 808 nm laser became stronger, confirming that the photothermal effect could improve the efficiency of the Fenton-like reaction. In normal conditions, the Cu-MNCS-AIPH@PAA + laser group showed obvious green fluorescence, demonstrating the production of alkyl radicals from APIH decomposition triggered by the photothermal effect. In simulated TEM, the strongest green fluorescence could be seen from the Cu-MNCS-AIPH@PAA + laser group, which was attributed to the more free radical production caused by the enhanced CDT and the decomposition of AIPH assisted by the photothermal effect. In addition, hemolysis experiments were performed to further verify the blood compatibility of Cu-MNCS-AIPH@PAA (Fig. S9, ESI†). When various concentrations of Cu-MNCS-AIPH@PAA were incubated with red blood cells, no significant hemolysis was detected, presenting good blood-compatibility. All these results demonstrated that Cu-MNCS-AIPH@PAA could act as a potential candidate for highly efficient cancer treatment.

Owing to the excellent efficacy of tumor therapy *in vitro*, the antitumor effect of Cu-MNCS-AIPH@PAA *in vivo* was further evaluated on an RM-1 mouse tumor model. The tumor-bearing mice were randomly divided into five groups: (I) control group, (II) 808 nm laser, (III) Cu-MNCS-AIPH@PAA, (VI) Cu-MNCS@PAA + 808 nm laser, and (V) Cu-MNCS-AIPH@PAA + 808 nm laser. The temperature of the tumors in the treatment group increased sharply from 36 °C to 55 °C within 10 min under exposure to an 808 nm laser, which was much higher than that of the saline group (from 36 to 39 °C) (Fig. 5a and Fig. S10, ESI†). This indicated the good photothermal effect of Cu-MNCS@PAA *in vivo*. In light of the principles of the regulation of Jilin University for the care and use of laboratory animals, the tumor length of tumor-bearing mice did not exceed 15 mm. When the tumor length in the control group reached 15 mm on the 8th day of treatment, the mice were killed off and the treatment was ended. During our

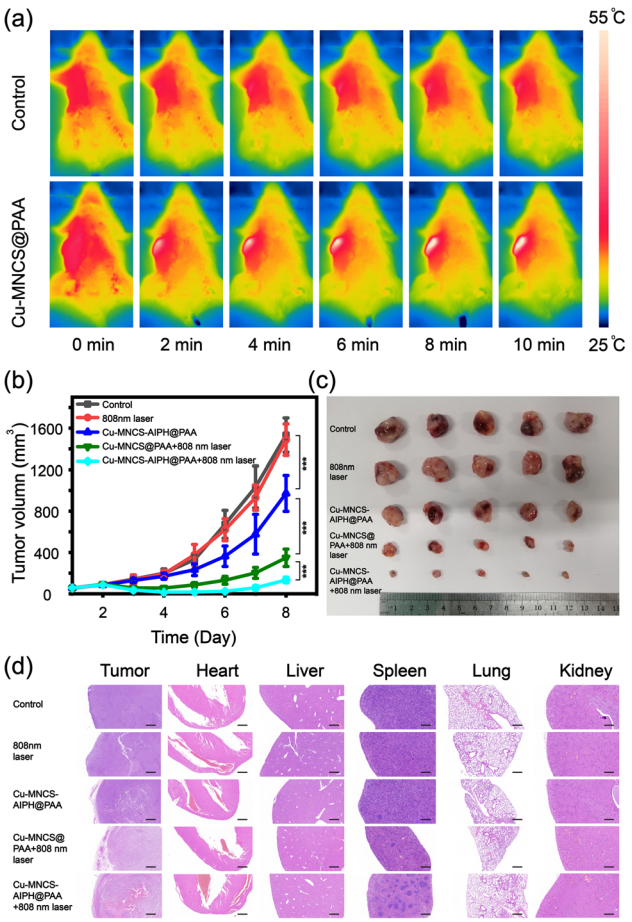

Fig. 5 (a) Thermal images *in vivo* after injection for 24 h. (b) Tumor volume after varied treatments (***$p < 0.001$). (c) Photos of final tumors. (d) H & E staining pictures of tumors and organs after different treatments (scale bar: 500 μm).

treatment, no obvious difference was noted in the body weight of the mice among different groups, which meant negligible acute toxicity of the nanoparticles (Fig. S11, ESI†). As shown in Fig. 5b, the control and laser groups displayed no obvious inhibition effect, and the Cu-MNCS-AIPH@PAA group showed a partial tumor inhibition effect owing to the •OH generation for CDT. The treatment efficiency of Cu-MNCS@PAA + 808 nm laser was noticeably enhanced, ascribed to the cooperative effect of PTT and CDT enhanced by the photothermal effect. More significant tumor growth suppression was observed in the Cu-MNCS-AIPH@PAA + 808 nm laser group (Fig. 5c and Fig. S12, ESI†), which meant an enhanced combination antitumor effect based on PTT, CDT and alkyl radical generation triggered by the photothermal effect. The histological analysis of major organs and tumor tissues further illustrated its good treatment effect (Fig. 5d). The results of blood routine examination and blood biochemistry examination after intravenous injection of Cu-MNCS-AIPH@PAA on the 30th day proved that Cu-MNCS-AIPH@PAA had low long-term toxicity *in vivo* (Fig. S13, ESI†).

Conclusions

To sum up, the novel nanoplatform Cu-MNCS-AIPH@PAA has been successfully prepared, which achieved highly efficient therapy of PCa through the cooperative effect of PTT, CDT, and alkyl radical generation triggered by the photothermal effect. The high conversion efficiency could not only make Cu-MNCS-AIPH@PAA serve as a good photothermal agent for PTT, but also improve the •OH generation efficiency through Fenton-like reaction and promote the decomposition of AIPH to produce alkyl radicals. The tumor growth was effectively suppressed by synergistic therapy of CDT, PTT, and alkyl radicals both *in vivo* and *in vitro*. Furthermore, Cu-MNCS-AIPH@PAA exhibited good biocompatibility and low long-term toxicity, which highlighted its great potential in clinical applications. The excellent anticancer efficiency and high biocompatibility enabled Cu-MNCS-AIPH@PAA to act as a promising nanoplatform for PCa therapy.

Conflicts of interest

There are no conflicts to declare.

Acknowledgements

This work was supported by the Program of Science and Technology Development Plan of Jilin Province of China (No. 20210101287JC), the Science and Technology Research Project of the Education Department of Jilin Province (JJKH20211189KJ), and the Jilin Province Medical and Health Talents Special Project.

Notes and references

1 H. Sung, J. Ferlay, R. L. Siegel, M. Laversanne, I. Soerjomataram, A. Jemal and F. Bray, *Ca-Cancer J. Clin.*, 2021, **71**, 209–249.
2 R. L. Siegel, K. D. Miller and A. Jemal, *Cancer statistics*, 2020, **70**, 7–30.
3 R. M. Hoffman, *N. Engl. J. Med.*, 2011, **365**, 2013–2019.
4 N. Fossati, P. M. Willemse, T. V. D. Broeck, R. C. N. V. D. Bergh, C. Y. Yuan, E. Briers, J. Bellmunt, M. Bolla, P. Cornford, M. D. Santis, E. MacPepple, A. M. Henry, M. D. Mason, V. B. Matveev, H. G. V. D. Poel, T. H. V. D. Kwast, O. Rouvière, I. G. Schoots, T. Wiegel, T. B. Lam, N. Mottet and S. Joniau, *Eur. Urol.*, 2017, **72**, 84–109.
5 D. P. Petrylak, C. M. Tangen, M. H. A. Hussain, P. L. Jr, J. A. Jones, M. E. Taplin, P. A. Burch, D. Berry, C. Moinpour, M. Kohli, M. C. Benson, E. J. Small, D. Raghavan and E. D. Crawford, *N. Engl. J. Med.*, 2004, **351**, 1513–1520.
6 N. G. Zaorsky, A. S. Harrison, E. J. Trabulsi, L. G. Gomella, T. N. Showalter, M. D. Hurwitz, A. P. Dicker and R. B. Den, *Nat. Rev. Urol.*, 2013, **10**, 565–579.
7 A. J. Chang, K. A. Autio, M. Roach III and H. I. Scher, *Nat. Rev. Clin. Oncol.*, 2014, **11**, 308–323.
8 C. Jia, Y. Guo and F. Wu, *Small*, 2022, **18**, e2103868.
9 C. Zhang, W. Bu, D. Ni, S. Zhang, Q. Li, Z. Yao, J. Zhang, H. Yao, Z. Wang and J. Shi, *Angew. Chem., Int. Ed.*, 2016, **55**, 2101–2106.
10 Z. Tang, Y. Liu, M. He and W. Bu, *Angew. Chem., Int. Ed.*, 2019, **58**, 946–956.
11 P. Ma, H. Xiao, C. Yu, J. Liu, Z. Cheng, H. Song, X. Zhang, C. Li, J. Wang, Z. Gu and J. Lin, *Nano Lett.*, 2017, **17**, 928–937.
12 S. Wang, Z. Wang, G. Yu, Z. Zhou, O. Jacobson, Y. Liu, Y. Ma, F. Zhang, Z. Y. Chen and X. Chen, *Adv. Sci.*, 2019, **6**, 1801986.
13 Z. Tang, P. Zhao, H. Wang, Y. Liu and W. Bu, *Chem. Rev.*, 2021, **121**, 1981–2019.
14 S. Ji, B. Jiang, H. Hao, Y. Chen, J. Dong, Y. Mao, Z. Zhang, R. Gao, W. Chen, R. Zhang, Q. Liang, H. Li, S. Liu, Y. Wang, Q. Zhang, L. Gu, D. Duan, M. Liang, D. Wang, X. Yan and Y. Li, *Nat. Catal.*, 2021, **4**, 407–417.
15 M. Huo, L. Wang, Y. Chen and J. Shi, *Nat. Commun.*, 2017, **8**, 357.
16 L. Chudal, N. K. Pandey, J. Phan, O. Johnson, L. Lin, H. Yu, Y. Shu, Z. Huang, M. Xing, J. P. Liu, M. L. Chen and W. Chen, *ACS Appl. Bio Mater.*, 2020, **3**, 1804–1814.
17 J. Kim, H. R. Cho, H. Jeon, D. Kim, C. Song, N. Lee, S. H. Choi and T. Hyeon, *J. Am. Chem. Soc.*, 2017, **139**, 10992–10995.
18 M. R. Junttila and F. J. D. Sauvage, *Nature*, 2013, **501**, 346–354.
19 W. Li, C. Su, Y. Chang, Y. Lin and C. Yeh, *ACS Nano*, 2016, **10**, 2017–2027.
20 W. Wang, Y. Jin, Z. Xu, X. Liu, S. Z. Bajwa, W. S. Khan and H. Yu, *Wiley Interdiscip. Rev.: Nanomed. Nanobiotechnol.*, 2020, **12**, e1614.
21 L. Fu, Y. Wan, C. Qi, J. He, C. Li, C. Yang, H. Xu, J. Lin and P. Huang, *Adv. Mater.*, 2021, **33**, e2006892.
22 S. Jin, L. Weng, Z. Li, Z. Yang, L. Zhu, J. Shi, W. Tang, W. Ma, H. Zong and W. Jiang, *J. Mater. Chem. B*, 2020, **8**, 4620–4626.
23 Y. Su, X. Zhang, G. Ren, Z. Zhang, Y. Liang, S. Wu and J. Shen, *Chem. Eng. J.*, 2020, **400**, 125949.

24 G. Liu, J. Zhu, H. Guo, A. Sun, P. Chen, L. Xi, W. Huang, X. Song and X. Dong, *Angew. Chem., Int. Ed.*, 2019, **58**, 18641–18646.
25 W. L. Wang, Z. Guo, Y. Lu, X. C. Shen, T. Chen, R. T. Huang, B. Zhou, C. Wen, H. Liang and B. P. Jiang, *ACS Appl. Mater. Interfaces*, 2019, **11**, 17294–17305.
26 P. Liu, Y. Wang, L. An, Q. Tian, J. Lin and S. Yang, *ACS Appl. Mater. Interfaces*, 2018, **10**, 38833–38844.
27 K. Xu, Y. Cheng, J. Yan, Y. Feng, R. Zheng, X. Wu, Y. Wang, P. Song and H. Zhang, *Nano Res.*, 2019, **12**, 2947–2953.
28 A. D. Bokare and W. Choi, *J. Hazard. Mater.*, 2014, **275**, 121–135.
29 X. Lu, S. Gao, H. Lin, L. Yu, Y. Han, P. Zhu, W. Bao, H. Yao, Y. Chen and J. Shi, *Adv. Mater.*, 2020, **32**, e2002246.
30 Q. Zou, M. Abbas, L. Zhao, S. Li, G. Shen and X. Yan, *J. Am. Chem. Soc.*, 2017, **139**, 1921–1927.
31 C. Guo, H. Yu, B. Feng, W. Gao, M. Yan, Z. Zhang, Y. Li and S. Liu, *Biomaterials*, 2015, **52**, 407–416.
32 L. Li, L. H. Rashidi, M. Yao, L. Ma, L. Chen, J. Zhang, Y. Zhang and W. Chen, *Photodiagn. Photodyn. Ther.*, 2017, **19**, 5–14.
33 H. Min, Y. Qi, Y. Zhang, X. Han, K. Cheng, Y. Liu, H. Liu, J. Hu, G. Nie and Y. Li, *Adv. Mater.*, 2020, **32**, e2000038.
34 J. Bai, X. Jia, W. Zhen, W. Cheng and X. Jiang, *J. Am. Chem. Soc.*, 2018, **140**, 106–109.
35 F. Liu, L. Lin, S. Sheng, C. Xu, Y. Wang, Y. Zhang, D. Wang, J. Wu, Y. Li, H. Tian and X. Chen, *Nanoscale*, 2020, **12**, 1349–1355.
36 Q. Zhang, Q. Guo, Q. Chen, X. Zhao, S. J. Pennycook and H. Chen, *Adv. Sci.*, 2020, **7**, 1902576.
37 F. Liu, L. Lin, Y. Zhang, Y. Wang, S. Sheng, C. Xu, H. Tian and X. Chen, *Adv. Mater.*, 2019, **31**, e1902885.
38 Y. Liu, W. Zhen, Y. Wang, J. Liu, L. Jin, T. Zhang, S. Zhang, Y. Zhao, S. Song, C. Li, J. Zhu, Y. Yang and H. Zhang, *Angew. Chem., Int. Ed.*, 2019, **58**, 2407–2412.
39 Z. Deng, C. Fang, X. Ma, X. Li, Y. J. Zeng and X. Peng, *ACS Appl. Mater. Interfaces*, 2020, **12**, 20321–20330.
40 G. Guan, X. Wang, B. Li, W. Zhang, Z. Cui, X. Lu, R. Zou and J. Hu, *Nanoscale*, 2018, **10**, 17902–17911.
41 S. Lei, J. Chen, K. Zeng, M. Wang and X. Ge, *Nano Res.*, 2019, **12**, 1071–1082.
42 Q. Chen, X. Shan, S. Shi, C. Jiang, T. Li, S. Wei, X. Zhang, G. Sun and J. Liu, *J. Mater. Chem. B*, 2020, **8**, 4056–4066.
43 Z. Liu, X. Zhao, B. Yu, N. Zhao, C. Zhang and F. J. Xu, *ACS Nano*, 2021, **15**, 7482–7490.
44 Z. Liu, C. Hu, S. Liu, L. Cai, Y. Zhou and M. Pang, *J. Mater. Chem. B*, 2021, **9**, 3295–3299.
45 H. Xiang, H. Lin, L. Yu and Y. Chen, *ACS Nano*, 2019, **13**, 2223–2235.
46 Y. Sun, D. Zhao, G. Wang, Y. Wang, L. Cao, J. Sun, Q. Jiang and Z. He, *Acta Pharm. Sin. B*, 2020, **10**, 1382–1396.
47 Y. Yoshida, N. Itoh, Y. Saito, M. Hayakawa and E. Niki, *Free Radical Res.*, 2004, **38**, 375–384.
48 J. Yang, R. Xie, L. Feng, B. Liu, R. Lv, C. Li, S. Gai, F. He, P. Yang and J. Lin, *ACS Nano*, 2019, **13**, 13144–13160.
49 Y. Li, H. Yu, J. Ren, G. Lu, Y. Cao, Z. Xu, Y. Kang and P. Xue, *Small*, 2022, **18**, e2104302.
50 L. Feng, S. Gai, Y. Dai, F. He, C. Sun, P. Yang, R. Lv, N. Niu, G. An and J. Lin, *Chem. Mater.*, 2018, **30**, 526–539.
51 X. Zheng, Y. Jin, X. Liu, T. Liu, W. Wang and H. Yu, *Bioact. Mater.*, 2021, **6**, 4301–4318.
52 G. Huang, Y. Qiu, F. Yang, J. Xie, X. Chen, L. Wang and H. Yang, *Nano Lett.*, 2021, **21**, 2926–2931.
53 S. Zuo, D. Li, Z. Guan, F. Yang, D. Xia and M. Huang, *Carbon*, 2022, **187**, 207–215.
54 X. Liu, D. Gregurec, J. Irigoyen, A. Martinez, S. Moya, R. Ciganda, P. Hermange, J. Ruiz and D. Astruc, *Nat. Commun.*, 2016, **7**, 13152.
55 P. A. Prakash, J. Liu, H. M. Lin and H. T. Chang, *J. Mater. Chem. A*, 2013, **1**, 5973–5981.